

# Direct Measurements of Heating by Electromagnetically Trapped Gold Nanoparticles on Supported Lipid Bilayers

Poul M. Bendix, S. Nader S. Reihani,<sup>†</sup> and Lene B. Oddershede\*

Niels Bohr Institute, University of Copenhagen, 2100 Copenhagen, Denmark. <sup>†</sup>Permanent address: IASBS, Zanjan, Iran.

**ABSTRACT** Absorption of electromagnetic irradiation results in significant heating of metallic nanoparticles, an effect which can be advantageously used in biomedical contexts. Also, metallic nanoparticles are presently finding widespread use as handles, contacts, or markers in nanometer scale systems, and for these purposes it is essential that the temperature increase associated with electromagnetic irradiation is not harmful to the environment. Regardless of whether the heating of metallic nanoparticles is desired or not, it is crucial for nanobio assays to know the exact temperature increase associated with electromagnetic irradiation of metallic nanoparticles. We performed direct measurements of the temperature surrounding single gold nanoparticles optically trapped on a lipid bilayer, a biologically relevant matrix. The lipid bilayer had incorporated fluorescent molecules which have a preference for either fluid or gel phases. The heating associated with electromagnetic radiation was measured by visualizing the melted footprint around the irradiated particle. The effect was measured for individual gold nanoparticles of a variety of sizes and for a variety of laser powers. The temperatures were highly dependent on particle size and laser power, with surface temperature increments ranging from a few to hundreds of degrees Celsius. Our results show that by a careful choice of gold nanoparticle size and strength of irradiating electromagnetic field, one can control the exact particle temperature. The method is easily applicable to any type of nanoparticle for which the photothermal effect is sought to be quantified.

**KEYWORDS:** Gold nanoparticles · heating · optical trapping · molecular partitioning · photothermal effect · lipid bilayer

**O**wing to the plasmonic properties of gold nanoparticles, the absorption and scattering cross sections vary dramatically across the optical spectrum. Their high optical extinction makes gold nanoparticles useful as nonfading optical labels which has been demonstrated by detection of single gold nanoparticles as small as 2.5 nm in biological environments.<sup>1–3</sup> Gold nanoparticles are extensively used for nanoengineering purposes to assist the self-assembly of DNA into three-dimensional architectures<sup>4</sup> or to allow remote release from liposomes.<sup>5</sup> While gold nanoparticles absorb predominantly in the visible spectral range a biological transparency window exists around near-infrared wavelengths<sup>6</sup> which has led to development of infrared resonant nanoparticles.<sup>7</sup> Gold nanoparticles

efficiently convert electromagnetic radiation into heat<sup>8</sup> and hence, they have potential in photothermal applications.<sup>7,9–11</sup> In particular, nanostructures with enhanced IR absorption, like gold nanorods, have proven promising for photothermal cancer therapy and gene delivery.<sup>12</sup>

With the extensive use of irradiated gold nanoparticles to investigate or manipulate biological specimens it is crucial to know the exact temperature profile around the particle. Different approaches have been applied to measure the optical heating of nanoparticles; the vaporization of surrounding liquid,<sup>13</sup> the melting of glass surfaces,<sup>8</sup> or the melting around gold nanoparticles embedded in ice<sup>14</sup> have been used as measures, however, these types of experiments are typically performed either with high energy pulsed lasers yielding extreme transient heating or in a matrix and at a temperature which is far from biologically relevant. However, recently heating around metallic nanoparticles irradiated by 532 nm laser light has been shown to induce reversible phase transitions in biologically relevant lipid bilayer systems.<sup>15</sup> In that and several other studies, calculations incorporating estimates of physically relevant parameters constituted an essential part of finding the temperature profile surrounding the irradiated particle.<sup>14,15,16</sup>

The strong interaction of metallic nanoparticles with electromagnetic radiation also leads to a strong polarization of the particle, thus enabling efficient optical trapping of individual metallic nanoparticles.<sup>16–21</sup> Here, we present direct quantitative measurements of the heating associated with infrared optical trapping of spherical gold nanoparticles

\*Address correspondence to oddershede@nbi.dk.

Received for review December 2, 2009 and accepted March 24, 2010.

Published online April 6, 2010.  
10.1021/nn901751w

© 2010 American Chemical Society

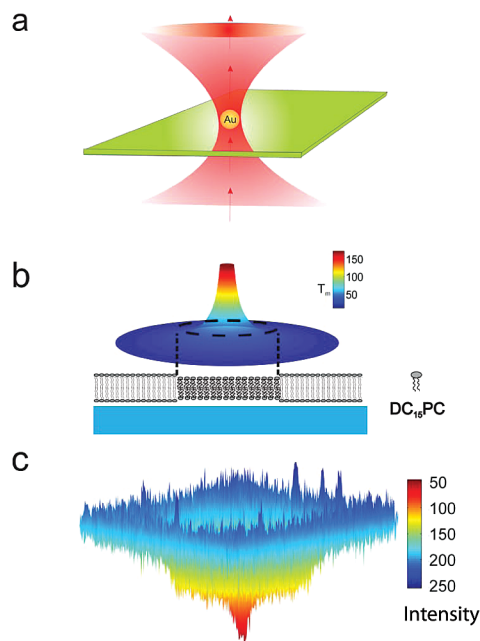


**Figure 1.** Illustration of the assay used to probe the nanoparticle temperature. (a) A gold nanoparticle adhered to a supported lipid bilayer is laterally positioned at the center of an optical trap. (b) The supported lipid bilayer (DC<sub>15</sub>PC) having a gel to fluid phase transition temperature slightly above room temperature serves as a biological sensor. If the temperature profile is as drawn, this will give rise to a melted region in the bilayer where the temperature is above  $T_m$ . The melted bilayer area is visualized using the lipophilic chromophore DiI<sub>C18</sub> which preferentially partitions into the gel phase. (c) Data showing the fluorescent emission from the vicinity of a  $d = 200$  nm gold nanoparticle using  $P = 120$  mW.

with diameters ranging from  $d = 80$  to  $d = 200$  nm. Our method makes no preassumptions about the system and only uses the very well characterized phase transitions of lipid bilayers. We directly show that the heating associated with infrared optical trapping of metallic nanoparticles ranges from a few degrees to hundreds of degrees Celsius, strongly depending on the size of the nanoparticle and the laser power.

## RESULTS AND DISCUSSION

**Molecular Partitioning as a Footprint of the Melted Region.** A sketch of the experiment is shown in Figure 1a. An optically trapped gold nanoparticle was fixed on a two-dimensional supported lipid bilayer (DC<sub>15</sub>PC). The temperature of the measurement chamber was 28 °C, and the phase transition of the bilayer occurred at 33 °C. If the temperature in the region around the optically trapped gold nanoparticle was elevated by more than 5 °C the lipid bilayer underwent a phase transition from the gel to the liquid disordered phase as sketched in Figure 1b. By selecting fluorophores with preference for either the fluid disordered phase or the tightly packed gel phase, we imaged the melted region by an increase or decrease in the fluorescent intensity, respectively. The chromophore DiI<sub>C18</sub> energetically favors the gel phase because of better hydrophobic matching be-

tween the hydrocarbon tails of the fluorescent probe and the longer lipid tails in the gel phase.<sup>22,23</sup> Figure 1c shows an example of fluorescent emission close to an optically trapped gold nanoparticle embedded in a lipid bilayer containing DiI<sub>C18</sub> which preferentially localizes in the gel phase. The intensity is significantly lower in the area surrounding the irradiated gold nanoparticle. In the fluid phase the molecules have a higher degree of rotational freedom and hence a reduced quantum yield. This effect further reduces the emission from the fluid region, thus improving the distinction of the fluid phase from the gel phase. We tested this molecular partition mechanism by also using Texas red labeled DPPE (TR-DPPE) lipids which are known to prefer fluid phases because of the presence of a bulky fluorophore conjugated to the PE headgroup.<sup>23–25</sup> As shown in Supporting Information Figure S1 and movie 1 we found TR-DPPE to be concentrated in an area surrounding the particle which equals the depleted area observed with DiI<sub>C18</sub> under the same conditions. The shorter analogue DiI<sub>C12</sub> was also observed to concentrate near the particle in the melted region (data not shown) in agreement with bulk data reported in ref 22.

**Quantification of Particle Temperatures.** The boundaries of the local phase transitions were quantified by calculating the area of the low intensity signatures on the surface. The recorded images were transformed into binary images with a threshold corresponding to the intensity of the gel phase bilayer. All pixels below the threshold value were assigned the value 1 and the surrounding pixels were assigned the value 0. The radius,  $r$ , of the melted zone was obtained from the measured area ( $= \pi r^2$ ) of the circular melted region. The area of the melted region strongly correlated with the particle size. As shown in Figure 2a particles having diameters 100 and 200 nm form fluid phases with diameters of  $\sim 1$  and  $\sim 10$   $\mu\text{m}$ , respectively, under same conditions. The fluorescent intensity along the dashed lines in Figure 2a are plotted in Figure 2b. A close inspection of Figure 2a,b shows that the footprint of the 200 nm particle appears to have two concentric circles, a smaller dark circle and a larger semidark circle; this effect is also visible on Figure 1c. The larger semidark circle is the melted footprint. The smaller darker circle probably is an effect of the high temperatures at the very center, the result of irradiating a large metallic particle with substantial laser power. This effect is not seen if the particle is only 100 nm in diameter and irradiated with 110 mW. The high temperature probably causes local damage to the fluorescent molecules in the bilayer. Also, the extreme temperatures near the particle lower the quantum yield of the fluorophores thus causing a further decrease in intensity.

The diameter of the melted region increased linearly with laser power. This is shown in Figure 3a where the diameter of the melted region is plotted as a function of laser power at the sample for gold nanoparticles

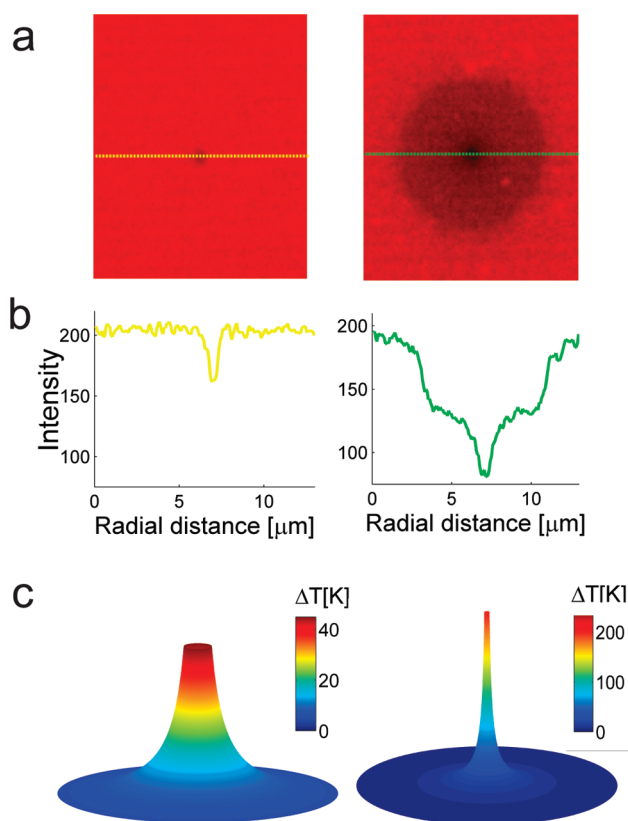


**Figure 2.** Quantification of the melted area and reconstruction of the temperature profile. Left part of the figure shows data from a trapped gold nanoparticle having  $d = 100$  nm, in the right part the particle has  $d = 200$  nm.  $P = 110$  mW. (a) The laser is irradiating the gold nanoparticle at the center of the picture. The melted region appears darker. (b) Intensity along the dotted lines in panel a. The size of the nanoparticle dramatically influences the extent of the melted region. (c) Temperature profiles reconstructed assuming a  $D^{-1}$  temperature dependence increase as in eq 1.

with diameters 80, 100, 150, and 200 nm. For each particle size we quantified the melted area for 10–15 particles for laser powers up to 425 mW; the error bars denote one standard deviation. The  $d = 200$  nm particles were pushed off the surface by the focused laser trap for laser powers exceeding 120 mW.

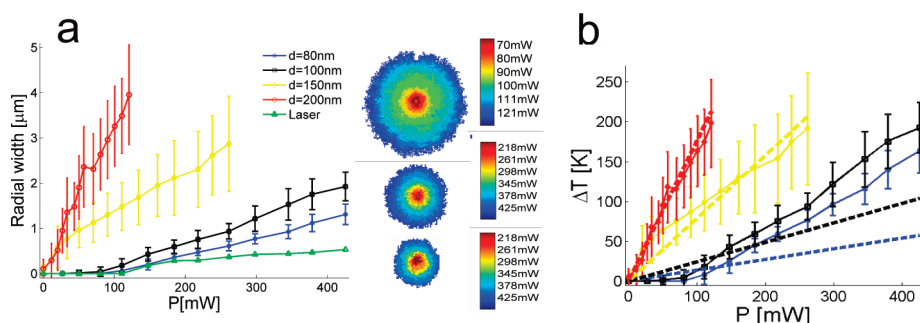


**Figure 3.** Quantification of surface temperatures of gold nanoparticles. (a) Diameter of the melted bilayer region as a function of laser power for different particle sizes:  $d = 200$  nm is shown with red circles,  $d = 150$  nm with yellow diamonds,  $d = 100$  nm with black squares, and  $d = 80$  nm with blue asterisks. The green triangles show the effect of the laser alone. (b) The temperature increase at the surface of the particle as a function of laser power for different particle sizes. The dashed lines are the temperature increases as predicted by a Mie calculation. The inset between graphs a and b shows examples of the standard deviation of the different measurements.

A quantitative description of the temperature increase around a sphere placed in an infinite medium is derived in ref 26 and is under steady state conditions given by

$$\Delta T(D) = \frac{R^3 A}{3DK} \quad (1)$$

where  $D$  is the distance from the particle center,  $R$  is the particle radius,  $K$  is the thermal conductivity of the surrounding medium, and  $A$  is the heating rate per unit volume given by  $A = I C_{\text{abs}}/V$ , with  $I$  being the power density at the particle location and  $V$  being the particle volume. For particles trapped with 1064 nm laser light, the absorption cross section,  $C_{\text{abs}}$ , of a particle with diameters larger than  $\approx 20$  nm is correctly calculated using Mie equations.<sup>15,27,28</sup> Cross sections calculated by this method using parameters which are relevant for the present study are plotted in Supporting Information, Figure S2 as a function of wavelength for various particle sizes.

For a particle of a given radius eq 1 can be rewritten as

$$\Delta T(D) = \frac{C I}{D} \quad (2)$$

where  $C$  is a constant including all the physical parameters which are difficult to determine correctly. Hence, the distance from the particle to the rim of the footprint,  $D_m$ , where the temperature is  $T(D_m) = T_m = 33$  °C, should have a linear relationship with the power incident on the particle,  $I$ . Using image analysis we quantified  $D_m$ , and Figure 3a shows  $D_m$  as a function of laser power. The relation is indeed linear thus verifying the relationship predicted by eqs 1 and 2. Fitting eq 2 to the data shown in Figure 3a allowed a determination of  $C$ . Using this value of  $C$  and the inverse relationship between  $\Delta T$  and  $D$  as predicted by eq 1 we were able to find the entire temperature profile surrounding the irradiated particle. The temperature increases at the surfaces of the nanoparticles as a function of particle size

and laser power is shown in Figure 3b, and examples of entire heating profiles for  $d = 100$  nm and  $d = 200$  nm are shown in Figure 2c. One of the strengths of the current approach is that we need not make any assumptions regarding the value of the absorption cross section, the thermal conductivity, or other relevant physical quantities. We experimentally found the heating at the surface of the  $d = 200$  nm particles to be 1640 K/W, of the 150 nm particles to be 732 K/W, of the 100 nm particles to be 452 K/W, and of the 80 nm particles to be 385 K/W.

The laser can bleach the bilayer by two-photon absorption, and heating due to absorption by water is also possible. To check the degree of these effects, an experiment was performed where the laser irradiated the lipid bilayer without any gold nanoparticles present. As shown in Figure 3a (green triangles) this caused the fluorescent intensity to decrease slightly in the focal region after some time of irradiation. Therefore, we only quantified particle temperatures which formed fluid regions larger than the signature formed by the focused laser. However, smaller particles having  $d = 60$  nm could be briefly irradiated to form fluid phases before the laser bleached the fluorescent molecules. The reflection from a laser-trapped 60 nm gold particle is shown in Figure 4c and the corresponding melted footprint is shown in Figure 4d (see also Supporting Information, movie 2).

In principle, this method can be used to reconstruct the temperature profile around any type of irradiated particle, for instance around an optically trapped micrometer-sized polystyrene particle. Polystyrene is a dielectric material with an absorption efficiency significantly smaller than gold. Hence, a polystyrene particle is expected to create a much smaller melted region than a similarly sized gold particle. This is demonstrated in Figure 4 panels a (fluorescent image) and b (melted footprint), where the melted region around an 800 nm polystyrene particle was observed to be significantly smaller than around a 60 nm gold particle (Figure 4c,d) under the same conditions. To achieve even greater sensitivity, the temperature of the sample was heated to 1 °C below the phase transition which resulted in a significantly larger melted region (compare the area in Supporting Information, Figure S3 to values given in Figure 3).

We also performed a theoretical calculation of the temperature profiles based on Mie equations. For  $K$  in eq 1 we used the thermal conductivity of water. This is only approximately correct as the glass coverslip has a slightly higher thermal conductivity than water and could cause additional heat flow not accounted for by eq 1. In our setup the bilayer provides some insulation between the particle and the glass. Also, the curved particle surface causes the contact area between the bilayer and the particle to be small, thus minimizing heat flow from the particle to the surface. Therefore, we ex-

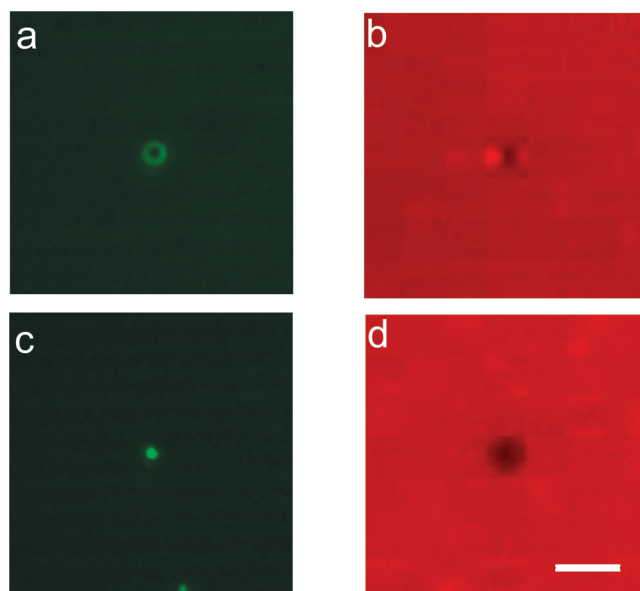
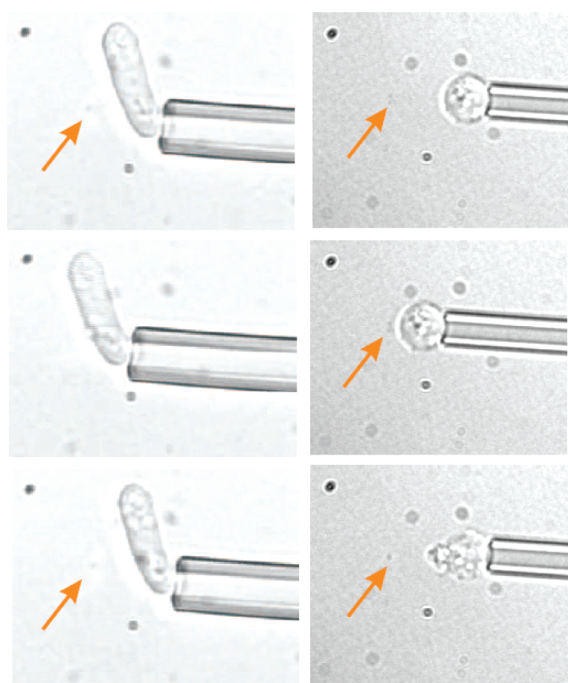


**Figure 4.** Optical heating of micrometer sized polystyrene particles and gold nanoparticles on DC<sub>15</sub>PC bilayers. (a) A fluorescent polystyrene particle,  $d = 800$  nm centered in the infrared laser beam. (b) Corresponding melting signature of the DiIC<sub>18</sub> labeled bilayer. (c) A  $d = 60$  nm gold nanoparticle centered in the infrared laser beam imaged in reflection mode. (d) Corresponding melting signature on the DiIC<sub>18</sub> labeled bilayer. Particles are irradiated by  $P = 298$  mW. Bar = 2  $\mu$ m.

pect the effect of the glass surface on the total heat conductivity to be small and for simplicity, we have chosen to neglect it in the calculation. The calculated surface temperatures are shown as dashed lines in Figure 3b (details of the calculations are given in the Supporting Information). The theoretically calculated heating at the surface is 1702 K/W for 200 nm, 792 K/W for 150 nm, 245 K/W for 100 nm, and 135 K/W for 80 nm particles. There is reasonable agreement between the experimentally determined values and the theoretically calculated values, in particular for the two largest particle sizes. In the Mie calculation the laser power was assumed to have a value which was an average across the Gaussian-shaped beam profile. This is probably not a valid assumption for the smaller particles, which, due to their small absorption cross section, experience a significantly larger laser intensity at the center of the beam.

In ref 16, the temperature profile around nanoparticles irradiated with 1064 nm focused laser light was calculated using the dipole approximation and indirectly confirmed through assumptions regarding various physical parameters. For a  $d = 100$  nm gold nanoparticle they found a heating of 266 K/W, which is below the value we directly measured for the same particle size (452 K/W) despite our larger focus. Apart from differences in experimental settings one important difference is that the heating measured in ref 16 was obtained indirectly by assuming that particle temperatures could be calculated using the dipole approximation, which does not account for the red shift and broadening of the plasmon band which has been



**Cell wall ablation**      **Membrane ablation**

**Figure 5.** Ablation of living cells using heating from optically trapped gold nanoparticles. Left column: a metabolically competent *Schizosaccharomyces pombe* yeast cell is held by a movable suction pipet and brought close to a stationary optically trapped gold nanoparticle (red arrow). Upon contact the heated particle,  $d = 200$  nm, disrupts the 150 nm thick glucan cell wall upon contact resulting in an osmotic bursting of the pressurized cell (see also Supporting Information, movie 4). Right column: a similar experiment with a protoplast formed by enzymatically degrading the cell wall of *Schizosaccharomyces pombe* yeast cells. Here, a trapped  $d = 100$  nm gold nanoparticle is used to disrupt the integrity of the protoplast membrane. The increased contrast in the optical trap in the lower right image is due to trapping of protoplasmic debris from the disrupted protoplast together with the gold particle.

measured in gold nanoparticles larger than  $d = 20$  nm.<sup>28</sup> In ref 15 a less focused green laser ( $\lambda = 532$  nm) was used to irradiate  $d = 80$  nm gold nanoparticles, and the surface temperature was estimated using a finite-element calculation. The absorption cross section at  $\lambda = 532$  nm is  $\sim 170$  times larger (see Supporting Information, Figure S2) than at  $\lambda = 1064$  nm used in the present study which, when accounted for, leads to a reasonable agreement between our direct measurements and the results in ref 15.

By direct measurements we determined temperatures at the surface of nanoparticles which by far exceeded the normal boiling point of water, however, without destabilizing the particle and without the observation of bubble formation. Nucleation of a bubble with radius  $r$  would require the vapor pressure to overcome the hydrostatic pressure as well as the surface pressure given by  $P_{\text{surf}} = 2\sigma/r$ , where  $\sigma = 70$  mN/m is the air/water surface tension. A nanoscale bubble having a radius of  $r = 100$  nm thus requires a vapor pressure of approximately 14 bar. At this pressure water boils at  $\sim 200$  °C. Larger nucleating bubbles are not re-

alistic since the temperature decreases by nearly 50% within a distance corresponding to the particle radius. This threshold temperature for bubble formation agrees well with the highest temperatures measured for  $d = 200$  nm particles before the particle escaped or explosive boiling occurred (see Figure 3b). Superheating up to 80–90% of the critical temperature of bulk water,  $T_c = 374$  °C, has been reported for smaller gold nanoparticles.<sup>13</sup> But eventually at high enough temperatures a thin insulating vapor layer will form and finally result in explosive boiling.<sup>13</sup> Increasing the temperature affects the density of the surrounding fluid. For water, for the maximum temperatures considered in the present study, the associated density increase is less than 10%. Also, the high temperatures only extend out to approximately a particle radius, whereas our measurements of the phase boundary were done several micrometers away from the particle. Hence, we believe this effect is negligible in comparison to the error bars on our results. Potentially, sonic shock waves could occur upon rapid heating, but in the experiment the laser power was slowly increased by a few mW between each acquired data point, and we never observed any such drastic effect.

**Controlled Heating in Biological Assays.** The experimentally determined heat profiles give useful information regarding possible applications of gold nanoparticles as nanoscale optical handles or as nanoscale heaters. To use optically trapped gold nanospheres as handles for probing biological systems, it is desirable to minimize particle size and laser power, hence minimizing the local temperature increase to a couple of degrees Celsius. To demonstrate that 40 nm particles can safely be used, we trapped streptavidin-coated 40 nm gold nanospheres conjugated to biotinylated lipids in a fluid lipid bilayer (see Supporting Information, movie 3). The particles diffused freely in 2D both before and after trapping indicating that the proximity of a strongly irradiated metal surface did not irreversibly affect the fluidity or structure of the bilayer.

For the use of laser irradiated gold nanoparticles as localized heat sources, it is encouraging that trapped particles with diameters larger than 100 nm can easily reach lethal temperatures for cells even several micrometers away from the particle surface. To demonstrate the use of gold nanoparticles as controlled local heat sources in a biological environment we optically trapped  $d = 200$  nm gold nanospheres and brought them into vicinity of metabolically competent *Schizosaccharomyces pombe* yeast cells, known to have an extremely stiff cell wall. Using a laser power of  $\sim 100$  mW at the sample we easily disrupted the cell wall thus causing cell death. One such experiment is shown in the left column of Figure 5 and Supporting Information, movie 4. Also, as shown in the right column of Figure 5 we used a  $d = 100$  nm particle held at  $\sim 100$  mW at the sample to ablate a softer protoplast.

## CONCLUSIONS

By using molecular partitioning and by exploiting the phase dependent quantum yield of fluorophores in lipid bilayers, we directly measured the heating associated with irradiation of gold nanoparticles. By utilizing the well established inverse linear relationship between temperature and distance to a heat source,<sup>26</sup> we mapped out the entire temperature profile surrounding individual irradiated gold nanoparticles. This was done without making any assumptions regarding the value of the absorption cross section, the thermal conductivity of the system, or other relevant physical quantities. The temperature increase was largely dependent on the irradiating laser power and on the size of the nanoparticle, the temperature increase ranging from undetectable to hundreds of degrees Celsius. The method uses a biologically relevant matrix, is easily performed at biologically relevant temperatures, and

is straightforward to apply to other types of nanoparticles. Controlled heating and visualizations of the melted area on a scale far below the optical resolution provides control over lipid phase transitions on a nanoscale. The phase coexistence region resulting from the well-controlled temperature gradient can be useful for studying dynamics of phase boundaries as well as partitioning behavior of lipophilic molecules between lipid phases consisting of one lipid component. In particular, our results pave the way for using optically heated nanoparticles in sensitive biological experiments or in medical applications like localized photothermal treatment of malignant cells.<sup>3,9,10</sup> Owing to the interesting photothermal response of novel nanostructures like gold nanorods,<sup>12</sup> these hold particular promise for such treatments, and future investigations will aim at quantifying heating profiles of individual rods.

## EXPERIMENTAL SECTION

**Lipid Assay.** For the lipid bilayer assay where fluorophores partitioned in the gel phase we used DC<sub>15</sub>PC (Avanti Polar lipids) with 5 mol % DiIC<sub>18</sub> fluorophores. Small unilamellar vesicles were allowed to fuse to a hydrophilic glass surface for 3 h at 37 °C above the gel-to-fluid phase transition.<sup>29</sup> Gel phase bilayers shrink around 20–25% upon cooling through the phase transitions,<sup>30</sup> which can potentially lead to cracks in the bilayers. Incorporation of a low percentage of positively charged DiIC<sub>18</sub> fluorophores improved the stability of the gel phase bilayer to resist cracking upon cooling through the phase transition.<sup>31</sup> Lipids suspended in chloroform were dried on glass under nitrogen flow and further dried in vacuum for 2 h. The lipid film was hydrated in PBS buffer at 37 °C. To form small unilamellar vesicles, we extruded the hydrated lipid mass through 100 nm filters at 37 °C. The vesicles contained 5 mol % of lipophilic fluorophores (DiIC<sub>18</sub> 1,1'-dioctadecyl-3,3,3',3'-tetramethylindocarbocyanine perchlorate, Molecular Probes) (emission maximum, 569 nm). Subsequently, the surfaces were thoroughly washed with Milli-Q water. To investigate partitioning of fluorescent lipophilic molecules into the fluid region, we used 3 mol % of Texas-red-labeled DPPE (Molecular Probes). All experiments were performed in PBS buffer at 100 mM NaCl, pH = 7.0. Glass surfaces were etched in piranha solution (3:1 sulfuric acid and hydrogen peroxide) for 30 min.

**Optical Trapping and Fluorescent Detection.** The optical trap was based on an Nd:YVO<sub>4</sub> (5 W Spectra Physics Millennia  $\lambda = 1064$  nm, TEM<sub>00</sub>) laser coupled into the back port of a Leica confocal laser scanning microscope (SP5/TCS). The laser was focused through a high numerical aperture oil immersion objective (HCX, PL, APO, 100 $\times$ , NA = 1.4, oil). To improve trapping, the collimated beam slightly overfilled the back aperture of the objective. The position of the focus was accurately positioned, with nanometer precision, relative to the surface using a three-dimensional piezoelectric stage (PI 731.20, Physik Instrumente, Germany). The laser focus was displaced in the axial direction from the optical focus of the microscope to simulate the configuration while trapping a gold nanoparticle in solution. The gold nanoparticles were imaged by collecting the back scattered light from the 514 nm laser line.<sup>32</sup> Particles with  $d = 40$  nm appeared darker than the background due to a dominant destructive interference between the background light and the light scattered by the particle, while the larger particles appeared brighter due to dominant scattering from the particles relative to the background.<sup>32,20</sup> Scattered light from the particle and fluorescent light from the bilayer were collected simultaneously using

two photomultiplier tubes. The chambers were heated using a custom built stage with water circulating from a temperature controlled water bath with a temperature stability of approximately 0.5 °C. The laser power reaching the objective was measured using a power meter and the transmission through the objective was measured with the dual objective method.<sup>33</sup> The spot size in the plane of the lipid bilayer was measured to be  $d_{\text{spot}} = 1.8 \mu\text{m}$  by bleaching an area on a fluorescently labeled gel phase bilayer cooled to 13 °C below the phase transition temperature. We used the maximum output to bleach the molecules in the focal region. The frozen bilayer exhibits very slow diffusion of fluorophores, and hence the bleached area represents the approximate extent of the focus. The average intensity,  $I$ , of the laser spot was approximated as  $I = 4P/\pi d_{\text{spot}}^2$ , where  $P$  is the total power delivered at the sample.

**Acknowledgment.** We are grateful for discussions with and advice from A. Kyrsting and L.B.O. acknowledges support from University of Copenhagen excellence grant.

**Supporting Information Available:** Calculation of absorption cross section; supplementary Figure S1 shows molecular partitioning using different fluorophores, supplementary Figure S2 shows absorption and extinction cross sections, supplementary Figure S3 shows a more sensitive assay, movie 1 visualizes heating induced molecular partitioning from a 200 nm particle, movie 2 visualizes heating induced molecular partitioning from a 60 nm gold nanoparticle, movie 3 demonstrates that no irreversible damage is done to the bilayer, and movie 4 shows ablation of a living cell. This material is available free of charge via the Internet at <http://pubs.acs.org>.

## REFERENCES AND NOTES

- Boyer, D.; Tamarat, P.; Maali, A.; Lounis, B.; Orrit, M. Photothermal Imaging of Nanometer-Sized Metal Particles Among Scatterers. *Science* **2002**, *297*, 1160–1163.
- Fujiwara, T.; Ritchie, K.; Murakoshi, H.; Jacobson, K.; Kusumi, A. Phospholipids Undergo Hop Diffusion in Compartmentalized Cell Membrane. *J. Cell. Biol.* **2002**, *157*, 1071–1082.
- McDougall, C.; Stevenson, D. J.; Brown, C. T. A.; Gunn-Moore, F.; Dholakia, K. Targeted Optical Injection of Gold Nanoparticles into Single Mammalian Cell. *J. Biophoton* **2009**, *2*, 736–743.

- Sharma, J.; Chhabra, R.; Cheng, A.; Brownell, J.; Liu, Y.; Yan, H. Control of Self-Assembly of DNA Tubules Through Integration of Gold Nanoparticles. *Science* **2009**, *323*, 112–116.
- Volodkin, D. V.; Skirtach, A. G.; Mohwald, H. Near-IR Remote Release from Assemblies of Liposomes and Nanoparticles. *Angew. Chem.* **2009**, *48*, 1809.
- Weissleder, R. A Clearer Vision for *in Vivo* Imaging. *Nat. Biotechnol.* **2001**, *19*, 316–317.
- Liu, H.; Chen, D.; Tang, F.; Du, G.; Li, L.; Meng, X.; Liang, W.; Zhang, Y.; Teng, X.; Li, Y. Photothermal Therapy of Lewis Lung Carcinoma in Mice Using Gold Nanoshells on Carboxylated Polystyrene Spheres. *Nanotechnology* **2008**, *19*, 455101.
- Numata, T.; Tatsuta, H.; Morita, Y.; Otani, Y.; Umeda, N. Localized Thermal Processing with a Laser-Trapped and Heated Metal Nanoparticle. *IEEE Trans.* **2007**, *2*, 398–401.
- El-Sayed, I. H.; Huang, X.; El-Sayed, M. A. Selective Laser Photothermal Therapy of Epithelial Carcinoma Using Anti-EGFR Antibody Conjugated Gold Nanoparticles. *Cancer Lett.* **2006**, *239*, 129–135.
- Zharov, V. P.; Galitovskaya, E. N.; Johnson, C.; Kelly, T. Synergistic Enhancement of Selective Nanophotothermolysis with Gold Nanoclusters: Potential for Cancer Therapy. *Laser Surg. Med.* **2002**, *37*, 219–226.
- Huang, X. H.; El-Sayed, I. H.; Qian, W.; El-Sayed, M. A. Cancer Cell Imaging and Photothermal Therapy in Near-Infrared Region by Using Gold Nanorods. *J. Am. Chem. Soc.* **2006**, *128*, 2115–2120.
- Huang, H.-C.; Barua, S.; Kay, D. B.; Rege, K. Simultaneous Enhancement of Photothermal Stability and Gene Delivery Efficacy of Gold Nanorods Using Polyelectrolytes. *ACS Nano* **2009**, *3*, 2941–2952.
- Kotaidis, V.; Dahmen, C.; Plessen, G.; Springer, F.; Plecha, A. Excitation of Nanoscale Vapor Bubbles at the Surface of Gold Nanoparticles in Water. *J. Chem. Phys.* **2006**, *124*, 184702.
- Richardson, H. H.; Nickman, Z. N.; Govorov, A. O.; Thomas, A. C.; Zhang, W.; Kordesch, M. E. Thermo-optical Properties of Gold Nanoparticles Embedded in Ice: Characterization of Heat Generation and Melting. *Nano Lett.* **2006**, *6*, 783–788.
- Urban, A. S.; Fedoruk, M.; Horton, M. R.; Radler, J. O.; Stefani, F. D.; Feldmann, J. Controlled Nanometric Phase Transitions of Phospholipid Membranes by Plasmonic Heating of Single Gold Nanoparticles. *Nano Lett.* **2009**, *9*, 2903–2908.
- Seol, Y.; Carpenter, A. E.; Perkins, T. T. Gold Nanoparticles: Enhanced Optical Trapping and Sensitivity Coupled with Significant Heating. *Opt. Lett.* **2006**, *31*, 2429–2431.
- Svoboda, K.; Block, S. M. Optical Trapping of Metallic Rayleigh Particles. *Opt. Lett.* **1994**, *19*, 930–932.
- Hansen, P. M.; Bhatia, V. K.; Harrit, N.; Oddershede, L. Expanding the Optical Trapping Range of Gold Nanoparticles. *Nano Lett.* **2005**, *5*, 1937–1942.
- Selhuber-Unkel, C.; Zins, I.; Schubert, O.; Soennichsen, C.; Oddershede, L. B. Quantitative Optical Trapping of Single Gold Nanorods. *Nano Lett.* **2008**, *8*, 2998–3003.
- Bosanac, L.; Aabo, T.; Bendix, P. M.; Oddershede, L. B. Efficient Optical Trapping and Visualization of Silver Nanoparticles. *Nano Lett.* **2008**, *8*, 1486–1491.
- Hajjizadeh, F.; Reihani, S. N. S. Optimized Optical Trapping of Gold Nanoparticles. *Opt. Express* **2010**, *18*, 551–559.
- Klausner, R. D.; Wolf, D. E. Selectivity of Fluorescent Lipid Analogs for Lipid Domains. *Biochemistry* **1980**, *19*, 6199–6203.
- Baumgart, T.; Hunt, G.; Farkas, E. R.; Webb, W. W.; Feigenson, G. W. Fluorescence Probe Partitioning Between Lo/Ld Phases in Lipid Membranes. *Biochim. Biophys. Acta* **2007**, *1768*, 2182–2194.
- Dietrich, C.; Bagatolli, L. A.; Volovyk, Z. N.; Thompson, N. L.; Levi, M.; Jacobson, K.; Gratton, E. Lipid Rafts Reconstituted in Model Membranes. *Biophys. J.* **2001**, *80*, 1417–1428.
- Veatch, S. L.; Keller, S. L. Separation of Liquid Phases in Giant Vesicles of Ternary Mixtures of Phospholipids and Cholesterol. *Biophys. J.* **2003**, *85*, 3074–3083.
- Goldenberg, H.; Tranter, C. J. Heat Flow in an Infinite Medium Heated by a Sphere. *Br. J. Appl. Phys.* **1952**, *3*, 296–298.
- Mie, G. Beitrage zur Optik Truber Medien, Speziell Kolloidaler Metallösungen. *Leipzig, Ann. Phys.* **1908**, *25*, 377–445.
- Kreibig, U.; Vollmer, M. In *Optical Properties of Metal Clusters*; Springer Series in Materials Science, Vol. 25; Springer: Berlin, 1995.
- Castellana, E. T.; Cremer, P. S. From Biophysical Studies to Sensor Design. *Surf. Sci. Rep.* **2006**, *61*, 429–444.
- Needham, D.; Evans, E. Structure and Mechanical Properties of Giant Lipid (DMPC) Vesicle Bilayers From 20 °C below to 10 °C above the Liquid Crystal-Crystalline Phase Transition at 24 °C. *Biochemistry* **1988**, *27*, 8261–8269.
- Zhang, L.; Spurlin, T. A.; Gewirth, A. A.; Granick, S. Electrostatic Stitching in Gelphase Supported Phospholipid Bilayers. *J. Phys. Chem. B* **2005**, *110*, 33–35.
- Jacobsen, V.; Stoller, P.; Brunner, C.; Vogel, V.; Sandoghdar, V. Interferometric Optical Detection and Tracking of Very Small Gold Nanoparticles at a Water–Glass Interface. *Opt. Express* **2006**, *14*, 405–414.
- Misawa, H.; Koshioka, M.; Sasaki, K.; Kitamura, N.; Masuhara, H. Three-Dimensional Optical Trapping and Laser Ablation of a Single Polymer Latex Particle in Water. *J. Appl. Phys.* **1991**, *70*, 3829–3836.